

**The relaxation matrix for symmetric tops with inversion symmetry. I. Effects of line coupling on self-broadened  $v_1$  and pure rotational bands of  $\text{NH}_3$**

Q. Ma and C. Boulet

Citation: *The Journal of Chemical Physics* **144**, 224303 (2016); doi: 10.1063/1.4952995

View online: <http://dx.doi.org/10.1063/1.4952995>

View Table of Contents: <http://scitation.aip.org/content/aip/journal/jcp/144/22?ver=pdfcov>

Published by the [AIP Publishing](#)

---

**Articles you may be interested in**

[The relaxation matrix for symmetric tops with inversion symmetry. II. Line mixing effects in the  \$v\_1\$  band of  \$\text{NH}\_3\$](#)

*J. Chem. Phys.* **144**, 224304 (2016); 10.1063/1.4952996

[Synchrotron-based far infrared study of the rotation-vibration-inversion spectrum of silacyclobutane below 500  \$\text{cm}^{-1}\$ : The  \$v\_{29}\$  and  \$v\_{30}\$  bands](#)

*J. Chem. Phys.* **139**, 244305 (2013); 10.1063/1.4848676

[Investigation of J dependence of line shift, line broadening, and line narrowing coefficients in the  \$v\_1 + 3v\_3\$  absorption band of acetylene](#)

*J. Chem. Phys.* **114**, 3535 (2001); 10.1063/1.1333022

[Investigation of line broadening in the  \$v\_1 + 3v\_3\$  band of acetylene](#)

*AIP Conf. Proc.* **467**, 503 (1999); 10.1063/1.58394

[Collisional self-broadening, shifting, and line-coupling of rotational transitions of  \$\text{CH}\_3\text{F}\$  in presence of Stark fields](#)

*AIP Conf. Proc.* **386**, 365 (1997); 10.1063/1.51875

---

**Ready, set, simulate.**

**REGISTER FOR THE COMSOL CONFERENCE >>**



# The relaxation matrix for symmetric tops with inversion symmetry. I. Effects of line coupling on self-broadened $\nu_1$ and pure rotational bands of $\text{NH}_3$

Q. Ma<sup>1</sup> and C. Boulet<sup>2</sup>

<sup>1</sup>NASA/Goddard Institute for Space Studies and Department of Applied Physics and Applied Mathematics, Columbia University, 2880 Broadway, New York, New York 10025, USA

<sup>2</sup>Institut des Sciences Moléculaires d'Orsay (ISMO), CNRS, Univ. Paris-Sud, Université Paris-Saclay, Bât. 350, Campus d'Orsay F-91405, France

(Received 15 March 2016; accepted 17 May 2016; published online 9 June 2016)

The Robert-Bonamy formalism has been commonly used to calculate half-widths and shifts of spectral lines for decades. This formalism is based on several approximations. Among them, two have not been fully addressed: the isolated line approximation and the neglect of coupling between the translational and internal motions. Recently, we have shown that the isolated line approximation is not necessary in developing semi-classical line shape theories. Based on this progress, we have been able to develop a new formalism that enables not only to reduce uncertainties on calculated half-widths and shifts, but also to model line mixing effects on spectra starting from the knowledge of the intermolecular potential. In our previous studies, the new formalism had been applied to linear and asymmetric-top molecules. In the present study, the method has been extended to symmetric-top molecules with inversion symmetry. As expected, the inversion splitting induces a complete failure of the isolated line approximation. We have calculated the complex relaxation matrices of self-broadened  $\text{NH}_3$ . The half-widths and shifts in the  $\nu_1$  and the pure rotational bands are reported in the present paper. When compared with measurements, the calculated half-widths match the experimental data very well, since the inapplicable isolated line approximation has been removed. With respect to the shifts, only qualitative results are obtained and discussed. Calculated off-diagonal elements of the relaxation matrix and a comparison with the observed line mixing effects are reported in the companion paper (Paper II). *Published by AIP Publishing.* [<http://dx.doi.org/10.1063/1.4952995>]

## I. INTRODUCTION

Retrieval of reliable information from space and ground-based measurements and the ability to perform reliable climate and atmospheric modelings require accurate knowledge of the spectroscopic parameters of all the significant molecules.<sup>1</sup> A complete knowledge of the corresponding lines, including how their shapes vary with the temperature and pressure of the atmospheric environment, is crucial in all of these applications. Usually, this knowledge is given by spectroscopic parameters for each of the transitions (i.e., the line position, the intensity, the self- and air-broadened half-widths, the shift, and the temperature exponent) that are stored in databases.<sup>2</sup> Among all the parameters, to accurately determine the last four is the most difficult problem that remains as a challenge for experimentalists and theorists. Because the ambient atmospheric species, temperatures, and pressures are not always amenable to laboratory measurements, or because of the large number of transitions, one often has to largely rely on theoretical calculations based on various line shape theories.<sup>1,3–8</sup>

The formalism developed by Robert and Bonamy<sup>7</sup> in 1979, based on the well-known Anderson-Tsao-Curnutte (ATC) theory,<sup>4,8</sup> is one of the most widely used methods, especially for complex molecules. Mainly due to its importance for practical applications, a lot of efforts have been made in order to improve the RB formalism (see Refs. 9 and 10

for a detailed presentation. However, so far its performance is still not satisfactory as it has been shown that in comparison with the measurements and the most accurate close coupling calculations, it significantly overestimates the half-widths.<sup>11,12</sup>

Although the non diagonality in the line space of the Liouville scattering operator was known,<sup>13,14</sup> a major limitation of the RB formalism results from applying nevertheless the isolated line approximation. Attempts to overcome this weakness take a long journey. Around 12 years ago, we have found that when the authors of Ref. 7 applied the linked cluster theorem to evaluate the Liouville scattering  $\hat{S}$  operator, there was a subtle derivation error and consequently, their expressions for operators (i.e.,  $S_1$  and  $S_2$ ) appearing in the cumulant expansion were not correct.<sup>15</sup> Unfortunately, after correcting this error we simply adopted their assumption that one needs only to consider diagonal matrix elements for operators involved in the cumulant expansion. It turns out that the latter is nothing, but the isolated line approximation. Mainly due to this negligence, an opportunity to completely remove this approximation was missed by us. In 2013, we finally realized that this approximation is not necessary because with the correct expressions, the matrix size of  $-iS_1 - S_2$  is dramatically reduced.<sup>10</sup> Thus, one can accurately evaluate the matrix elements of  $\exp(-iS_1 - S_2)$ , and consequently, calculate the whole relaxation matrix based on the potential energy surfaces between the molecules involved. It then

became possible to analyze line mixing effects for complex molecular systems for which fully quantum approach are not feasible.

In our previous studies, we have developed a refined formalism applicable for linear<sup>16–18</sup> and asymmetric-top molecules.<sup>19</sup> In the present study, the method has been extended to symmetric-top molecules with inversion symmetry where the relatively small inversion splitting induces a complete failure of the isolated line approximation and results in significant line coupling within doublets. As an example, we have applied the refined method to the calculation of the relaxation matrices for self-broadened NH<sub>3</sub>.

The pressure broadening of NH<sub>3</sub> lines has been the subject of numerous experimental and theoretical studies, mainly due to its importance for tropospheric and planetary atmosphere studies. Besides, it is the simplest molecule with inversion symmetry. Half-widths and shifts in the  $\nu_1$  band were measured by Markov *et al.* in 1993 for some selected lines.<sup>20</sup> In 1994, Brown and Peterson<sup>21</sup> measured half-widths in the pure rotational R branch between 40 and 210 cm<sup>-1</sup>, and developed empirical formulas. The latter have been used to complete the HITRAN data base. In 2004, Pine and Markov<sup>22</sup> have improved their earlier results by considering profiles more sophisticated than the Voigt profile. There are many other measurements carried out in  $\nu_2$ ,  $2\nu_2$ ,  $\nu_3$ , and  $\nu_4$  bands by different groups.<sup>23–26</sup>

On the other hand, previous theoretical calculations were mainly carried out based on the ATC or RB formalisms.<sup>24,25,27–30</sup> In the present work, we have applied our refined formalism to the calculation of the self-broadened half-widths and shifts in the  $\nu_1$  and the pure rotational bands. The results are reported here as well as the derivation of the formalism. In the companion paper, calculated off-diagonal elements of the relaxation matrix and a comparison with the observed effects of line mixing are reported.<sup>31</sup>

Independently, Cherkasov<sup>32</sup> has proposed a different approach. In his formalism, the scattering operator is also put into an exponential form without relying on the cumulant expansion, but in contrast with us, his operator  $-iS_1 - S_2$  does depend on the states of the bath molecules and consequently, has a corresponding space of huge dimension. The difficulty in evaluating matrix elements of  $\exp(-iS_1 - S_2)$  forces him to introduce additional approximations. Recently, he has applied his method to Q(j,k) doublets in the  $\nu_1$  band of self-broadened NH<sub>3</sub> and has demonstrated that the isolated line approximation is not applicable.<sup>33</sup> By comparing his numerical calculations with ours, there are other differences. For example, the linespace he considered is limited to a  $2 \times 2$  matrix constructed within each inversion doublet. This implies that in the whole relaxation matrix, all the off-diagonal elements are zero unless the two lines of interest belong to the same doublet. As we will report in Paper II,<sup>31</sup> this statement may be wrong. Indeed, intradoublet off-diagonal elements are not always negligible and could be comparable in magnitude with other off-diagonal ones.

## II. THEORY

### A. Basis sets of the symmetric-top absorber with inversion symmetry in the line space

It is well known that the wave functions of a symmetric-top molecule labeled as  $|jkm\rangle$  are  $\sqrt{(2j+1)/8\pi^2} D_{mk}^{j*}(\alpha, \beta, \gamma)$  where  $D_{mk}^j(\alpha, \beta, \gamma)$  are rotational matrices. In order to have definite parity, it is necessary to introduce the parity adapted wave functions defined by

$$|v\varepsilon jkm\rangle = N_\varepsilon (|v j k m\rangle + \varepsilon |v j - k m\rangle), \quad (1)$$

where  $k = 0, 1, \dots, j$  and for  $k = 0$ ,  $N_\varepsilon = 1, \varepsilon = 0$ ; for  $k \neq 0$ ,  $N_\varepsilon = 1/\sqrt{2}$ . With respect to the index  $\varepsilon$  for  $k \neq 0$ , we adopt the definition given by Green<sup>34</sup> such that  $\varepsilon = \pm(-1)^{j+1}$  where  $\varepsilon = (-1)^{j+1}$  and  $\varepsilon = (-1)^j$  correspond to the symmetric vibrational inversion (i.e., “s”) and the anti-symmetric vibrational inversion (i.e., “a”), respectively. In Eq. (1), a short notation  $v$  is used to represent all vibrational quantum numbers. We follow Ben-Reuven’s conventions<sup>35</sup> and introduce a set of bases  $|v_i \varepsilon_i j_i k_i v_f \varepsilon_f j_f k_f, J M_J\rangle$  in the line space defined by

$$\begin{aligned} & |v_i \varepsilon_i j_i k_i v_f \varepsilon_f j_f k_f, J M_J\rangle \\ &= \sum_{m_i m_f} (-1)^{j_f - m_f} C(j_i j_f J, m_i - m_f M_J) \\ & \times |v_i \varepsilon_i j_i k_i m_i v_f \varepsilon_f j_f k_f\rangle. \end{aligned} \quad (2)$$

In order to simplify notations, we will sometimes adopt a simple notation of  $i$  to represent all the quantum numbers of  $v_i, \varepsilon_i, j_i$ , and  $k_i$ .

In the present study, the bath molecule of interest will be a symmetric top. With respect to its states, we use a simple notation of  $|i_2 m_2\rangle$  where  $i_2$  is a short notation to represent all the quantum numbers in its ground state except for the magnetic quantum number  $m_2$ . Because one usually assumes that the bath molecule remains in the vibrational ground states, the notation  $i_2$  represents the parity  $\varepsilon_2$ , the angular momentum  $j_{i_2}$ , and its component  $k_2$  along the  $z$  axis in the molecular fixed frame. Thus,  $|i_2 m_2\rangle$  means  $|\varepsilon_2 j_{i_2} k_2 m_2\rangle$ . For simplifying symbols, the angular momentum  $j_{i_2}$  is denoted by  $j_2$  later.

### B. Expression for matrix elements of the relaxation operator

Following procedures detailed in Refs. 10 and 15–19, matrix elements of the relaxation operator can be expressed in terms of the average of the Liouville scattering operator over the internal degrees of the bath molecule, expressed via a second order cumulant expansion as

$$\begin{aligned} W_{i'f',if} &= \frac{n_b \bar{v}}{2\pi c} \int_{r_{c,min}}^{+\infty} 2\pi \left( b \frac{db}{dr_c} \right) dr_c \\ & \times \left\{ \delta_{i'f'} \delta_{f'f} - \langle \langle i'f' | e^{-iS_1(r_c) - S_2(r_c)} | if \rangle \rangle \right\} \end{aligned} \quad (3)$$

where  $n_b$  is the number density of the bath molecules,  $\bar{v}$  is the averaged velocity,  $b$  is the impact parameter, and  $r_c$  is the distance of closest approach for a given trajectory.

### C. Expressions for matrix elements of $S_1$ and $S_2$

With the semi-classical line shape theories,<sup>4,7-9</sup> the matrix elements of the first and second order operators  $S_1$  and  $S_2$  can be calculated from the intermolecular potential. For systems consisting of two symmetric-top molecules, the potential can be expressed in terms of a spherical tensor expansion as<sup>36</sup>

$$V(\vec{R}(t)) = \sum_{L_1 K_1 L_2 K_2 L} U(L_1 L_2 L; K_1 K_2; R(t)) \times \sum_{\mu_1 \mu_2 M} C(L_1 L_2 L, \mu_1 \mu_2 M) D_{\mu_1 K_1}^{L_1*}(\Omega_a) \times D_{\mu_2 K_2}^{L_2*}(\Omega_b) Y_{LM}^*(\omega(t)), \quad (4)$$

where the  $C(L_1 L_2 L, \mu_1 \mu_2 M)$  are Clebsch-Gordan coefficients and the  $D_{\mu K}^L(\Omega)$  are rotation matrices. The orientations of the absorber and bath molecules are described by  $\Omega_a$  and  $\Omega_b$ , respectively. The translational motion is described by  $R(t)$  and  $\omega(t)$ . The isotropic part of the potential  $V_{iso}$  corresponds to the component with  $L_1 = K_1 = L_2 = K_2 = 0$  in Eq. (4) and some time, it is represented by a fit to a 12-6 Lennard-Jones (LJ) form with two adjusted parameters  $\epsilon_{LJ}$  and  $\sigma_{LJ}$ .

As for the anisotropic part of the potential, it is here limited to the dipole-dipole ( $V_{dd}$ ), dipole-quadrupole ( $V_{dq}$ ), quadrupole-dipole ( $V_{qd}$ ), and quadrupole-quadrupole ( $V_{qq}$ ) components. Because the  $\text{NH}_3$  molecule has a very large dipole moment and a significant quadrupole moment, we expect that a combination of the leading multipole interactions represents the anisotropic potential sufficiently well. This approximation has been validated<sup>31</sup> by calculations.

According to the definition of  $S_1$ , its matrix elements are determined by the vibrational dependence of the isotropic potential through the following expression:

$$S_1^{i'f',if} = \frac{\delta_{i'i} \delta_{f'f}}{\hbar} \times \int_{-\infty}^{\infty} dt [\langle v_i | V_{iso}(t) | v_i \rangle - \langle v_f | V_{iso}(t) | v_f \rangle]. \quad (5)$$

In the present study, because there is no knowledge of the vibrational dependence of  $\epsilon_{LJ}$  and  $\sigma_{LJ}$  for the  $\text{NH}_3\text{-NH}_3$  system, we assume that the vibrational dependence of  $V_{iso}$  mainly comes from the isotropic induction and dispersion

components which are given by

$$V_{iso}^{ind} = -\frac{\mu_1^2 \alpha_2}{R^6} \quad (6)$$

and

$$V_{iso}^{disp} = -\frac{3U_1 U_2}{2(U_1 + U_2)} \times \frac{\alpha_1 \alpha_2}{R^6}, \quad (7)$$

respectively. Here,  $\mu_1$  is the dipole moment of the absorber molecule,  $\alpha_{1,2}$  are the isotropic polarizabilities of the absorber and bath molecules, and  $U_{1,2}$  the ionization energies. With the ‘‘exact’’ trajectory model,<sup>37,38</sup> a matrix element of  $S_1$  is given by

$$S_1(r_c)^{if,if} = \frac{2r_c}{\hbar v} \int_1^{\infty} x dx \times \frac{|\Delta V_{iso}(xr_c)|_{if}}{\left\{x^2 - 1 + \frac{2V_{iso}(r_c)}{mv^2} - x^2 \frac{2V_{iso}(xr_c)}{mv^2}\right\}^{\frac{1}{2}}}, \quad (8)$$

where  $\Delta V_{iso}$  denotes the vibration-dependent part of  $V_{iso}$ .<sup>39</sup>

With respect to the  $S_2$  term, it is usually divided into three terms:  $S_{2,outer,i}$ ,  $S_{2,outer,f}$ , and  $S_{2,middle}$  and we follow the same custom here. It is known that for linear molecules<sup>16-18</sup>  $S_{2,outer,i}$  and  $S_{2,outer,f}$  are diagonal (in the line space) and complex matrices while  $S_{2,middle}$  is an off-diagonal and real matrix. Note that similar properties were also observed, however, with different definitions of the  $S_2$  operators.<sup>13,14,32,40</sup> For more complicated molecules whose rotational states are labeled by additional quantum numbers besides the angular momentum  $j$ , the diagonality of  $S_{2,outer,i}$  and  $S_{2,outer,f}$  may not be valid. However, the reality and the non-diagonality of  $S_{2,middle}$  remain true. This implies that in contrast to linear molecules, one needs to provide more general expressions for  $S_{2,outer,i}$  and  $S_{2,outer,f}$  for symmetric tops.

Before deriving expressions for these terms, we would like to note that the formalism can be given in the standard or the symmetrized forms.<sup>16</sup> In the derivation presented here, we follow the symmetrized form where the density matrix  $\rho$  is symmetrized. It is easy to switch back to the standard form with a replacement of  $\sqrt{\rho_{i_2} \rho_{i_2'}}$  appearing in the following expressions by  $\rho_{i_2}$ . In addition, we note that we adopt a convention such that  $\rho_{i_2}$  does not include the degeneracy factor  $(2j_2 + 1)$ .

The derivations of these expressions and definitions of terms are presented in [Appendices A](#) and [B](#). With Eq. (B5), the expression for the real part of  $S_{2,outer,i}^{i'f',if}(r_c)$  is given by

$$\begin{aligned} \text{Re} S_{2,outer,i}^{i'f',if}(r_c) &= \pi \delta_{j_i' j_i} \delta_{f' f} \sum_{L_1 K_1 K_1' L_2 K_2 K_2'} \sum_{\epsilon_i'' j_i'' k_i''} (2j_i'' + 1) \\ &\times D^P(\epsilon_i' j_i' k_i', \epsilon_i'' j_i'' k_i''; L_1 K_1) D^P(\epsilon_i'' j_i'' k_i'', \epsilon_i j_i k_i; L_1 K_1) \sum_{i_2 i_2'} \sqrt{\rho_{i_2} \rho_{i_2'}} (2j_2 + 1) \\ &\times (2j_2' + 1) D^P(\epsilon_2 j_2 k_2, \epsilon_2' j_2' k_2'; L_2 K_2) D^P(\epsilon_2' j_2' k_2', \epsilon_2 j_2 k_2; L_2 K_2) \\ &\times \mathbb{F}_{L_1 K_1 K_1' L_2 K_2 K_2'} \left( \frac{\omega_{i_i''} + \omega_{i_i'}}{2} + \omega_{i_2 i_2'}, \omega_{i_i} \right). \end{aligned} \quad (9)$$

The expression for the imaginary part of  $S_{2,outer,i}^{i'f',if}(r_c)$  is the same as Eq. (9) except that  $\mathbb{F}_{L_1K_1K'_1L_2K_2K'_2}$  are replaced by  $\mathbb{H}_{L_1K_1K'_1L_2K_2K'_2}$ .

However, in many cases one does not need to calculate the off-diagonal elements of  $S_{2,outer}$ . For example, if the intermolecular potential does not contain components with  $K_1 \neq 0$ , the quantum numbers of  $k_i, k'_i, k''_i$  appearing in the  $D^P$

factors in Eq. (9) must be identical. This identity yields a factor of  $\delta_{k'_i k_i}$  and a combination of  $\delta_{j'_i j_i}$  and  $\delta_{k'_i k_i}$  implies that  $i'$  and  $i$  are the same states. Thus in this case, the operators  $S_{2,outer,i}$  and  $S_{2,outer,f}$  are diagonal matrices within a given vibrational band. Then, one can use simpler expressions to calculate their diagonal elements. More explicitly, the real part of a diagonal element of  $S_{2,outer,i}$  is given by

$$\begin{aligned} \text{Re}S_{2,outer,i}^{if,if}(r_c) &= \sqrt{\frac{\pi}{2}} \sum_{L_1K_1K'_1L_2K_2K'_2} \sum_{\varepsilon'_i j'_i k'_i} (2j'_i + 1) \\ &\times D^P(\varepsilon_i j_i k_i, \varepsilon'_i j'_i k'_i; L_1K_1) D^P(\varepsilon'_i j'_i k'_i, \varepsilon_i j_i k_i; L_1K'_1) \sum_{i_2 i'_2} \sqrt{\rho_{i_2} \rho_{i'_2}} (2j_2 + 1) (2j'_2 + 1) \\ &\times D^P(\varepsilon_2 j_2 k_2, \varepsilon'_2 j'_2 k'_2; L_2K_2) D^P(\varepsilon'_2 j'_2 k'_2, \varepsilon_2 j_2 k_2; L_2K'_2) \mathbb{F}_{L_1K_1K'_1L_2K_2K'_2}(\omega_{ii'} + \omega_{i_2 i'_2}). \end{aligned} \quad (10)$$

Note that in order to simplify notations, we use the same symbols of  $\mathbb{F}_{L_1K_1K'_1L_2K_2K'_2}$  to represent the 2-D and 1-D Fourier transforms in Eqs. (9) and (10). Readers can distinguish them by the number of their arguments. The expression of  $\text{Im}S_{2,outer,i}^{if,if}(r_c)$  together with those of  $\text{Re}S_{2,outer,f}^{if,if}(r_c)$  and  $\text{Im}S_{2,outer,f}^{if,if}(r_c)$  can be easily obtained from Eq. (10) by making proper replacements of  $\mathbb{F}_{L_1K_1K'_1L_2K_2K'_2}$  by  $\mathbb{H}_{L_1K_1K'_1L_2K_2K'_2}$  and/or exchanges between the quantum numbers  $i$  and  $f'$  and between  $i'$  and  $f$ .

As a next step, we consider the expression of  $S_{2,middle}$ . As mentioned above, the  $S_{2,middle}$  operator is always off-diagonal. With Eq. (C9), the expression of matrix elements  $S_{2,middle}^{i'f',if}$  is given by

$$\begin{aligned} S_{2,middle}^{i'f',if}(r_c) &= 2\pi(-1)^{1+J} \delta_{v'_i v_i} \delta_{v'_f v_f} (-1)^{j_f + j'_f} \\ &\times \sqrt{(2j'_i + 1)(2j'_f + 1)(2j_i + 1)(2j_f + 1)} \sum_{L_1K_1K'_1L_2K_2K'_2} (-1)^{L_1} W(j'_i j'_f j_i j_f, JL_1) \\ &\times D^P(\varepsilon'_i j'_i k'_i, \varepsilon_i j_i k_i; L_1K_1) D^P(\varepsilon_f j_f k_f, \varepsilon'_f j'_f k'_f; L_1K'_1) \\ &\times \sum_{i_2 i'_2} \sqrt{\rho_{i_2} \rho_{i'_2}} (2j_2 + 1) (2j'_2 + 1) D^P(\varepsilon'_2 j'_2 k'_2, \varepsilon_2 j_2 k_2; L_2K_2) D^P(\varepsilon_2 j_2 k_2, \varepsilon'_2 j'_2 k'_2; L_2K'_2) \\ &\times \mathbb{F}_{L_1K_1K'_1L_2K_2K'_2} \left( \frac{\omega_{i'i} + \omega_{f'f}}{2} + \omega_{i_2 i'_2}, \omega_{fi} - \omega_{f'i'} \right). \end{aligned} \quad (11)$$

For linear perturbors, one can consider them as special symmetric-top perturbors. By replacing  $D^P(\varepsilon_2 j_2 k_2, \varepsilon'_2 j'_2 k'_2; L_2K'_2)$  by  $C(j_2 j'_2 L_2, 000)$ ,  $D^P(\varepsilon'_2 j'_2 k'_2, \varepsilon_2 j_2 k_2; L_2K_2)$  by  $C(j'_2 j_2 L_2, 000)$ , and setting  $K_2 = K'_2 = 0$  in the Fourier transforms, Eqs. (9)–(11) become applicable for symmetric-top absorbers with inversion doubling immersed in a bath of linear molecules.

### III. PREPARATION OF THE CALCULATIONS

#### A. Selection of molecular parameters of $\text{NH}_3$ in the ground and $v_1$ states

For symmetric tops with inversion symmetry, the value of the doublet splitting is the most important factor to determine the effects of line coupling. For  $\text{NH}_3$ , one can directly obtain energy levels from databases such as HITRAN.<sup>2</sup> However, most of these values result from various and complex intramolecular resonances among numerous levels.<sup>41,42</sup> Of course, the present formalism neglects these resonances in the expression of the basis eigenvectors (Eqs. (1) and (2)), which are “0th” order wavefunctions. By making the same approximation, one can calculate them with simple formulas containing two sets of parameters. One set is applicable for states with the symmetric vibrational inversion

and another for the anti-symmetric vibrational inversion. For the fundamental vibrational state, these parameters are provided by Urban *et al.*<sup>43</sup> In general, the accuracy of calculated energy levels in the ground state is sufficient for our practical applications. For the  $v_1 = 1$  vibrational state, the two corresponding sets are provided by Angstl *et al.*<sup>44</sup> However, as is known from that work, rovibrational levels for  $v_1 = 1$  and  $j > 6$  are affected by strong intramolecular resonances, prohibiting the use of “0th” order formulas. Based on these considerations, we have decided to set  $j_{\max} = 8$  as the maximum of initial angular number for lines to be considered.

With respect to the other molecular parameters, the average dipole moment of  $\text{NH}_3$  in the ground and  $v_1$  states is 1.4719 and 1.4791 (in Debye), respectively.<sup>45</sup> The value of quadrupole moment (i.e.,  $Q = -2.32 \text{ D } \text{\AA}$ ) and the

polarizability associated with the ground state ( $\alpha = 2.18 \text{ \AA}^3$ ) come from Ref. 36. In order to calculate the  $S_1$  term with Eq. (7), one needs to know the value of  $\alpha_f - \alpha_i$ . With a formula provided by Russell and Spackman,<sup>46</sup> one can find  $\alpha_{1,f} - \alpha_{1,i} = 0.0445 \text{ \AA}^3$  (for comparison, Dhib *et al.*,<sup>27</sup> had selected  $\alpha_{1,f} - \alpha_{1,i} = 0.05 \text{ \AA}^3$  for the  $\nu_4$  band). Finally, the ionization energy of  $\text{NH}_3$  is  $U_1 = U_2 = 10.16 \text{ eV}$ .<sup>47</sup>

## B. Construction of linespaces

In general, the linespaces of interest are constructed by all the lines belonging to a given vibrational band. For vibrational bands of symmetric tops, the number of lines in a band can be over a thousand. Actions to handle such large size matrices not only once, but many times are not realistic. This implies that one has to find ways to divide the whole linespace into many smaller sub-linespaces. The smaller the sizes of these sub-blocks are, the easier are the calculations.

In the present study we only consider parallel bands of  $\text{NH}_3$  where the dipolar selection rules are  $\Delta j = 0, \pm 1$ ;  $\Delta k = 0$ ;  $a \leftarrow s, s \leftarrow a$ . At the same time, since  $\text{NH}_3$  has large dipole and quadrupole moments and the latter lie along its symmetric axis, the leading multipole interactions between two  $\text{NH}_3$  molecules have only spherical components with  $K_1 = 0$  and  $K_2 = 0$  in Eq. (4). This implies that the line coupling (cf. Eq. (11)) occurs only among lines with the same  $k$  values. As a result, the whole linespace can be divided into  $j_{\max} + 1$  sub-linespaces and consequently, the sizes of these sub-blocks are significantly reduced. With the cut-off  $j_{\max} = 8$ , the whole linespace to be considered is constructed from 217 lines. There are 9 sub-blocks associated with  $k = 0, 1, 2, \dots, 8$  whose sizes are 17, 46, 40, 34, 28, 22, 16, 10, and 4, respectively.

## C. Selections of the trajectory and potential models

Concerning the trajectory, we have adopted an “exact” model with trajectories governed by the isotropic potential.<sup>37,38,48</sup> In order to well sample all important trajectories, we have selected 600 values for the closest distance  $r_c$  with more dense points to depict nearly head-on collisions than other ones.

With respect to the potential, we assume that the isotropic part of the potential between two interacting  $\text{NH}_3$  molecules can be represented by the LJ model and the anisotropic part consists of the  $V_{dd}$ ,  $V_{dq}$ ,  $V_{qd}$ , and  $V_{qq}$  interactions. The two LJ parameters (i.e.,  $\sigma_{LJ} = 3.018 \text{ \AA}$  and  $\epsilon_{LJ} = 294.3 \text{ K}$ ) are adopted from Bouanich *et al.*<sup>49</sup> and these values are assumed to be independent of vibration modes.

## D. Calculations of the Fourier and Hilbert transforms

Based on the selected trajectory and potential models, one can calculate the corresponding 2-D and 1-D correlation functions. Given the fact that all of the  $V_{dd}$ ,  $V_{dq}$ ,  $V_{qd}$ , and  $V_{qq}$  interactions have no spherical components associated with  $K_1 \neq 0$  and  $K_2 \neq 0$  in Eq. (4) and that the  $\nu_1$  and pure rotational transitions do not involve any bending motions, only four 2-D and four 1-D correlation functions are required.

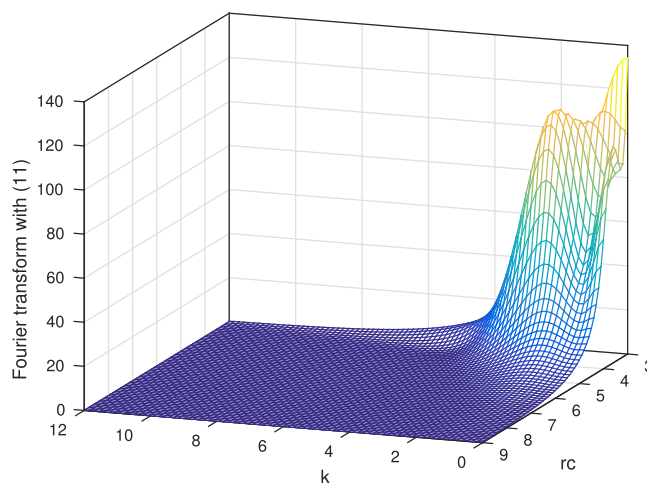


FIG. 1. The Fourier transform of  $\mathbb{F}_{100100}(k, r_c)$  (in  $\text{ps}^{-2}$ ) at  $T = 296 \text{ K}$  where  $k$  is dimensionless and  $r_c$  is given in  $\text{\AA}$ .

More explicitly, they are denoted as  $\mathbb{G}_{100100}$ ,  $\mathbb{G}_{100200}$ ,  $\mathbb{G}_{200100}$ , and  $\mathbb{G}_{200200}$  with two or one  $\tau$  arguments (cf. Appendix C). For simpler notation, they can be identified by values of the two ranks of  $L_1$  and  $L_2$  as (11), (12), (21), and (22).

Once these symmetric correlation functions are available, we introduce their causal partners which are identical to them for  $\tau \geq 0$  and are set to be zero for  $\tau < 0$ .<sup>50</sup> Then, we carry out the complex Fourier transforms of the 2-D and 1-D causal correlation functions and the real and imaginary parts of the results are just the symmetric 2-D and 1-D Fourier transforms and the subsequent 2-D and 1-D Hilbert transforms, respectively. Note that those associated with (11) are dominant.

Based on the LJ model, the minimum of closest distances for the “exact” trajectories at  $T = 296 \text{ K}$  is  $r_{c,\min} = 2.906 \text{ \AA}$ . In Fig. 1, we present a profile of the symmetric 1-D Fourier transform with (11) as a function of  $k$  and  $r_c$  in the range of  $[0, 12]$  and  $[3 \text{ \AA}, 9 \text{ \AA}]$  where  $k = (r_c \omega / \bar{v})$  is a dimensionless argument. Readers must be careful to distinguish this dimensionless  $k$  from the project quantum number  $k$  used to denote wave functions of  $\text{NH}_3$ . In Fig. 2,

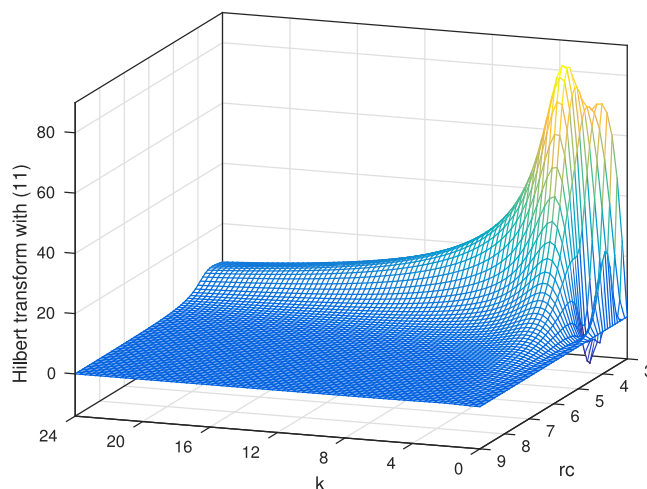


FIG. 2. The same as Fig. 1 except for the Hilbert transform of  $\mathbb{H}_{100100}(k, r_c)$ .

we present a profile of the 1-D Hilbert transform with (11). Meanwhile, given the fact that the symmetric Fourier transform is even over  $k$  and the Hilbert transform is odd, their ranges of  $k$  in these two plots are limited to  $k \geq 0$ . Finally, it is worth mentioning that if we plot these two transforms multiplied by a factor of  $(r_c/3.0)^6$ , their profiles remain identical for  $r_c > 6 \text{ \AA}$ . The variation with  $r_c$  as  $1/r_c^6$  is a well-known feature for these two transforms derived from the dipole-dipole interaction and the straight line trajectory model. For glancing collisions happening at large  $r_c$ , differences between the “exact” trajectory model and the straight line model are negligible.

The symmetric 2-D Fourier transforms are functions of the three arguments  $k$ ,  $k'$ , and  $r_c$ . To derive them is a large computational task, but one only needs to do it once. The calculated results can be stored as input files for the calculation of the off-diagonal elements of  $S_{2,\text{middle}}$ . In order to show their profiles, we present a three dimensional plot of the main function  $\mathbb{F}_{100100}(k, k', r_c)$  at  $r_c = 5.5 \text{ \AA}$  and  $T = 296 \text{ K}$  in Fig. 3. We have selected the trajectory with  $r_c = 5.5 \text{ \AA}$  to represent typical collisions beyond nearly head-on collisions because after  $r_c \geq 5.5 \text{ \AA}$ , all the trajectories become closer to a straight line. In addition, for the  $\text{NH}_3\text{-NH}_3$  system with strong dipole-dipole interaction, the glancing collisions are the dominant broadening and coupling processes. For the straight line trajectories, the magnitude of  $\mathbb{F}_{100100}(k, k', r_c)$  behaves as  $(1/r_c)^6$  and its dependences on  $k$  and  $k'$  remain unchanged. This implies that the conclusion drawn from analyzing Fig. 3 with  $r_c = 5.5 \text{ \AA}$  is valid for all other trajectories in this category. As shown in the figure,  $\mathbb{F}_{100100}(k, k', r_c \geq 5.5 \text{ \AA})$  has two peaks located near  $(1.05, 0)$  and  $(-1.05, 0)$  in the  $k$  and  $k'$  coordinates. Roughly speaking, for  $|k| \approx 4$  or  $|k'| \approx 4$ , its magnitude is around 14 times smaller than its maximum. Therefore, one can consider  $|k| = 4$  or  $|k'| = 4$  as a limitation such that as long as one of these two parameters is larger than this limit, the corresponding off-diagonal elements of  $S_{2,\text{middle}}$  become negligible. In terms of the dimensional parameters  $k$  and  $k'$ , the above conclusion is valid for all trajectories with  $r_c \geq 5.5 \text{ \AA}$ . These limits in  $k$ ,  $k'$  can be converted in  $\omega, \omega'$

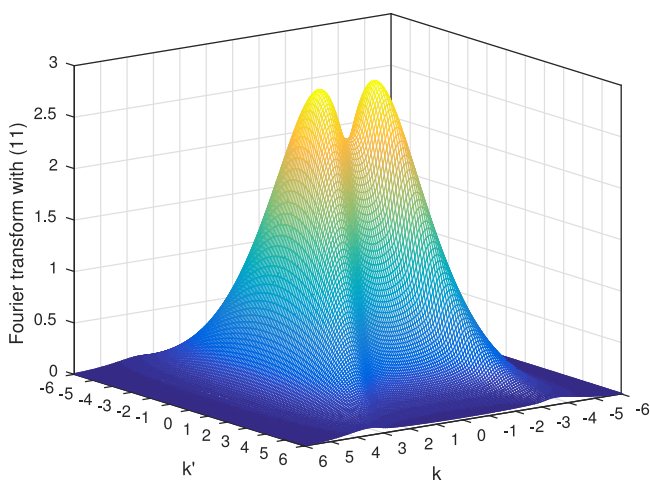


FIG. 3. The symmetric 2-D Fourier transform of  $\mathbb{F}_{100100}(k, k', r_c)$  (in  $\text{ps}^{-2}$ ) at  $r_c = 5.5 \text{ \AA}$  and  $T = 296 \text{ K}$  for the  $\text{NH}_3\text{-NH}_3$  system.

with a simple formula,  $\omega = 5.309 \left(\frac{\bar{v}}{r_c}\right) k$  where  $\bar{v}$  is in the units of  $10^4 \text{ cm/s}$  and  $r_c$  is in  $\text{\AA}$ . For example, for  $r_c = 5.5 \text{ \AA}$ , the limitation for both the  $|\omega|$  and  $|\omega'|$  is  $33 \text{ cm}^{-1}$  and for  $r_c = 7.0 \text{ \AA}$ , it is  $26 \text{ cm}^{-1}$ .

## E. Calculations of the matrix elements of $\exp(-iS_1 - S_2)$

After all matrix elements of  $S_1$  and  $S_2$  are available, the remaining problem is now to find a proper way to calculate matrix elements of the exponential of  $-iS_1 - S_2$ . The first step is to diagonalize the matrix  $-iS_1 - S_2$ , in order to obtain its complex eigenvalues and complex right (or left) eigenvectors. From the former, one constructs a diagonal matrix  $D$  and from the latter a right eigenvector matrix  $X_R$  whose columns represent the corresponding eigenvectors. Then, one finds the inverse matrix  $X_R^{-1}$ . Finally, the exponential of  $-iS_1 - S_2$  is given by

$$e^{-iS_1 - S_2} = X_R e^D X_R^{-1}. \quad (12)$$

## IV. CALCULATED HALF-WIDTHS

In the present study, the interaction potential does not connect lines with different  $k$  values. Calculations mentioned in Eqs. (10)–(12) are independently carried out for each of the sub-linespaces labeled by  $k$ .

### A. Two approximate rules applicable for calculated half-widths and shifts

It is well known that without including any vibrational dependences, calculated half-widths and shifts of  $\text{NH}_3$  lines from the ATC theory<sup>4</sup> or the RB formalism<sup>7</sup> have a symmetry applicable for two lines with switching their initial and final rotational states. In other words, for the pairs  $\{aR(j, k), sP(j+1, k)\}$ ,  $\{aQ(j, k), sQ(j, k)\}$ ,  $\{sR(j, k), aP(j+1, k)\}$ , and  $\{sQ(j, k), aQ(j, k)\}$ , the calculated half-widths are exactly identical while the shifts have exactly identical magnitudes, but opposite signs.

For the  $\nu_1$  band of  $\text{NH}_3$ , the vibrational dependence of both the average dipole moment and the spectroscopic parameters does exist, but they are not strong enough to completely break this symmetry down. In other words, the symmetry rules remain approximately valid. Our calculated results with considering the line coupling have confirmed the above conclusions: if vibrational dependences are ignored, these symmetries remain exact, and they are approximately valid in the case of the “real”  $\nu_1$  band.

Besides, there is an approximate rule applicable for two lines by only switching their initial and final inversion symmetry indices “s” and “a.” In other words, the widths are approximately equal for pairs of  $\{aP(j, k), sP(j, k)\}$  and  $\{aR(j, k), sR(j, k)\}$ , regardless of the inclusion or not of the line coupling in calculations. It is easy to understand this approximate symmetry because within the same pair, their differences only result from the inversion indices and in general, their doubling splits are small.

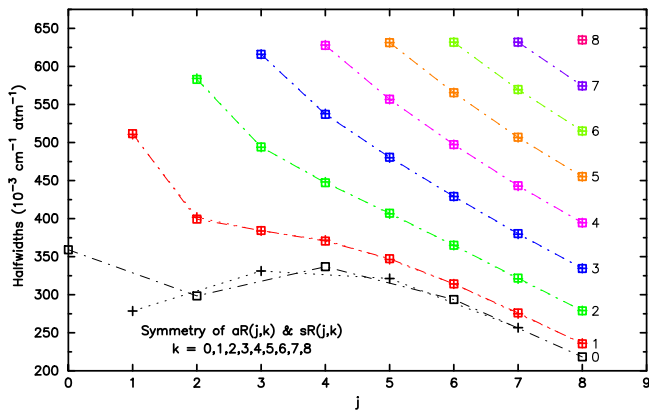


FIG. 4. An approximate symmetry of calculated half-widths for pairs of  $aR(j,k)$  ( $\square$ ) and  $sR(j,k)$  ( $+$ ) with  $k = 0, 1, 2, \dots, 8$ . The sub-blocks are labeled by their  $k$  value at the right side of  $aR(8,k)$  and symbols in a specified  $k$  sub-block are given in the same color and connected by a thin line.

In Fig. 4, we present calculated half-widths of  $aR(j, k)$  and  $sR(j, k)$  lines in the  $\nu_1$  band to show the second rule. Although these symmetry properties are approximate, one can use them as tools to check the consistency of calculated results and measured data because significant violations represent red flags.

## B. Overestimation of calculated half-widths due to the isolated line approximation

It is known that the RB formalism significantly overestimates the half-widths.<sup>11,12</sup> Recently we have demonstrated that for the systems  $N_2-N_2$ ,<sup>10</sup>  $C_2H_2-N_2$ ,<sup>17</sup>  $CO_2-N_2$ ,<sup>18</sup> and  $H_2O-N_2$ ,<sup>19</sup> removing the isolated line approximation reduces the calculated half-widths which get closer to measurements. In the present study, given the fact that except for those with  $k = 0$ , all the other  $NH_3$  lines are doublets having small splitting, the inapplicability of this assumption is well expected.

In Fig. 5, we present relative differences of half-widths of  $R(j,k)$  lines in the pure rotational band derived without and with the line coupling (L.C.). We do not distinguish  $sR(j,k)$  and  $aR(j,k)$  here because the difference is negligible. As shown

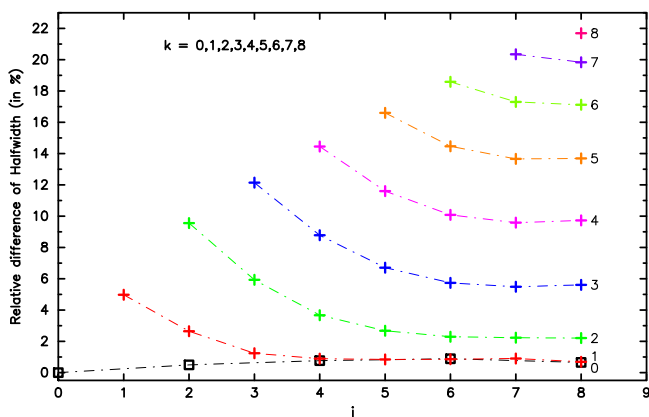


FIG. 5. Overestimation of calculated half-widths (i.e.,  $[\gamma_{noL.C.} - \gamma_{L.C.}] / \gamma_{L.C.}$ ) for  $R(j,k)$  lines in the pure rotational band resulting from the isolated line approximation.

in the plot, the relative difference for  $R(j,k)$  (in %) strongly depends on  $k$  and the larger the  $k$  is, the larger the reduction. Its value varies from almost zero at  $k = 0$  to more than 20% at  $k = 8$ . It is easy to understand why there are no reductions for  $R(j,0)$  because these lines do not have doubling partners. The reduction also varies with  $j$ , but it decreases as  $j$  increases from its maximum value for  $j = k$  to a constant value at higher  $j$ .

By removing the isolated line approximation, calculated half-width values are reduced and meanwhile, calculated relaxation matrices become non-diagonal. We note that a large reduction of the diagonal element of the  $n$ -th column (and  $n$ -th row) indicates that some off-diagonal elements of the corresponding column and row likely differ from zero by significant amounts. Because non-zero off-diagonal elements directly represent the line coupling, the reduction of the half-width of a line can serve as a measure of how strongly this line couples with others. Because the reduction variation pattern shown in Fig. 5 can be used to understand the line coupling pattern,<sup>31</sup> its investigation deserves a detailed analysis.

With our formalism, we can explain these  $k$  and  $j$  dependences. The non-diagonality of  $-iS_1 - S_2$  results solely from the off-diagonal elements of  $S_{2,middle}$  whose expression is given by Eq. (11). From Eq. (11), one can conclude that the coupling between two given lines is mainly determined by two factors. One is the coupling strength factor defined by

$$(-1)^{L_1} \sqrt{(2j'_i + 1)(2j'_f + 1)(2j_i + 1)(2j_f + 1)} \times W(j'_i j'_f j_i j_f, JL_1) D^P(\epsilon'_i j'_i k'_i, \epsilon_i j_i k_i; L_1 K_1) \times D^P(\epsilon_f j_f k_f, \epsilon'_f j'_f k'_f; L_1 K'_1), \quad (13)$$

and another is the 2-D Fourier transforms  $\mathbb{F}_{L_1 K_1 K'_1 L_2 K_2 K'_2}$  with two arguments of  $\frac{\omega_{i'i} + \omega_{f'f}}{2} + \omega_{i'i_2}$  called the energy gap and  $\omega_{f_i} - \omega_{f'_i}$  called the frequency gap in the following. The magnitudes of the off-diagonal elements of  $S_{2,middle}$  between two lines are thus governed by the coupling strength factor, the energy gap, and the frequency gap. In addition, the first factor plays the most important role because contributions are simply proportional to its magnitude. Concerning the two gaps, as

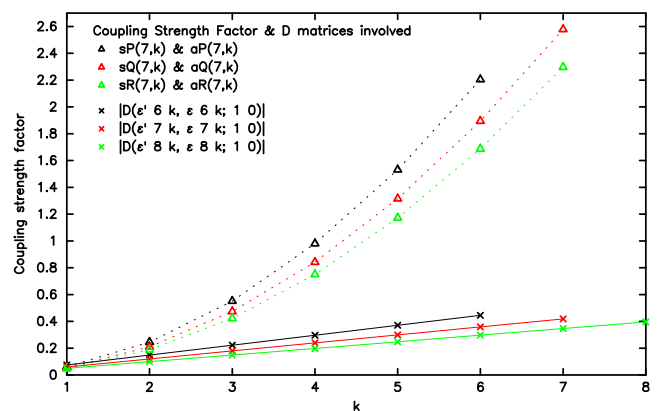


FIG. 6. The coupling strength factors of the doublets  $P(7,k)$ ,  $Q(7,k)$ , and  $R(7,k)$  and the  $D^P$  matrices involved (i.e.,  $D^P(\epsilon' 6 k, \epsilon 6 k; 1 0)$ ,  $D^P(\epsilon' 7 k, \epsilon 7 k; 1 0)$ , and  $D^P(\epsilon' 8 k, \epsilon 8 k; 1 0)$ ).

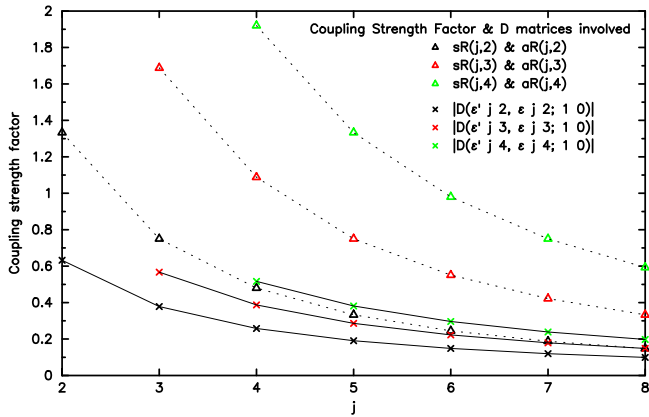


FIG. 7. The coupling strength factors of the doublets  $R(j,2)$ ,  $R(j,3)$ , and  $R(j,4)$  and the  $D^P$  matrices involved (i.e.,  $D(e' j 2, e j 2; 1 0)$ ,  $D(e' j 3, e j 3; 1 0)$ , and  $D(e' j 4, e j 4; 1 0)$ ).

shown by the profiles of  $\mathbb{F}_{L_1 K_1 K'_1 L_2 K_2 K'_2}$ , the smaller these two gaps are, the larger the magnitudes of  $\mathbb{F}_{L_1 K_1 K'_1 L_2 K_2 K'_2}$ .

For the  $\text{NH}_3$  molecule, its rotational constants are quite large. Except for doublets, the energy and frequency gaps between two lines are generally large. In contrast, values of these two gaps within doublets in the  $\nu_1$  and pure rotational bands are smaller than  $2 \text{ cm}^{-1}$ . Based on this fact, one can draw two conclusions. The first is, in most cases (not always), that the largest off-diagonal elements of  $S_{2,\text{middle}}$  are obtained for doublets. Besides, among these doublets, the amplitude of the off-diagonal elements of  $S_{2,\text{middle}}$  is mainly determined by the magnitude of the strength factor. In Fig. 6, we present magnitudes of the coupling strength factor for the doublets  $P(7,k)$ ,  $Q(7,k)$ , and  $R(7,k)$  as functions of  $k$ . As shown in the figure, roughly speaking, the magnitudes of the strength factor quadratically increase as  $k$  increases. This implies that the calculated off-diagonal elements of  $S_{2,\text{middle}}$  increase by the same amount. Meanwhile, variations of the diagonal elements remain within the same order. Thus, as  $k$  increases, the line coupling of these doublets becomes stronger and stronger. This is the reason why reduction of calculated half-widths quickly increases as  $k$  increases. Furthermore, according to Eq. (13), it is the  $D^P$  matrices involved that cause the  $k$  dependence described above. In order to demonstrate this, these  $D^P$  matrices are also plotted in Fig. 6. As can be seen, the magnitude of the  $D^P$  matrices roughly linearly increases with  $k$ , leading to the roughly quadratic increase of the strength factor.

Similarly, we can provide an explanation for the  $j$  dependence of the reductions of the calculated half-widths when line coupling is considered. Figure 7 gives the coupling strength factor for the doublets  $R(j,2)$ ,  $R(j,3)$ , and  $R(j,4)$  as functions of  $j$  together with the  $D^P$  matrices involved.

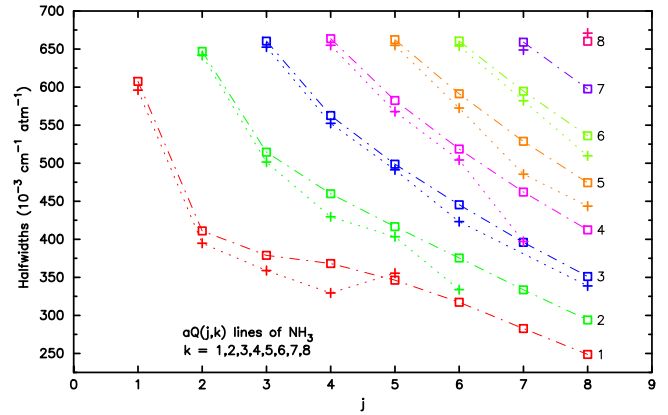


FIG. 8. Calculated half-widths ( $\square$ ) and measured results (+) by Pine and Markov<sup>22</sup> of  $sQ(j,k)$  lines in the  $\nu_1$  band. The sub-blocks are labeled by their  $k$  values on the right side of  $sQ(8,k)$  and symbols in a specified  $k$  sub-block are given in the same color and connected by a thin line.

The strong resemblance between the  $j$  variation patterns of the coupling strength factor in Fig. 7 and the reduction of half-width in Fig. 5 is clearly exhibited.

The case of the  $aR(0,0)$  line deserves a special comment. It has no doublet partner to which it can be coupled, but exhibits a very important shift as shown by Table I. Such a shift results from a very significant imaginary term of  $\text{Im}S_2$ , while  $S_1$  has a small influence. At the same time,  $\text{Im}S_2$  significantly modifies the calculation of the widths, even in the absence of any L.C. effect.

### C. Comparisons between calculated half-widths and measurements

In Fig. 8, we present comparisons between our calculated half-widths for  $sQ(j,k)$  and  $aQ(j,k)$  lines in the  $\nu_1$  band and the measured data by Pine and Markov.<sup>22</sup> As can be seen, the agreements are very good. Concerning the pure rotational band, we present a similar comparison between our calculated half-widths of  $sR(j,k)$  lines and Brown and Peterson's measurements<sup>21</sup> in Fig. 9. Very good agreements between the theory and measurements are also obtained. Comparisons for lines with the inversion “a” symmetry in these two bands are very similar to Figs. 8 and 9 are not presented here. Meanwhile, see the supplementary material<sup>51</sup> for detailed comparisons of calculated and experimental widths and shifts.

For other systems  $\text{N}_2\text{-N}_2$ ,  $\text{C}_2\text{H}_2\text{-N}_2$ , and  $\text{CO}_2\text{-N}_2$  previously studied,<sup>10,17,18</sup> although calculated half-widths were significantly reduced, the new results still differed from measurements by significant amounts. Removing only the isolated line approximation was not sufficient to match measurements. In contrast, the very good agreements obtained

TABLE I. Contributions to the half-width and shift (in  $10^{-3} \text{ cm}^{-1} \text{ atm}^{-1}$ ) from  $S_1$  and  $\text{Im}S_2$ .

$\Gamma$	Without L.C.		With L.C.		Experiment Ref. 22				
	Without $S_1$ and $\text{Im}S_2$	With $S_1$ and $\text{Im}S_2$	Without $S_1$ and $\text{Im}S_2$	With $S_1$ and $\text{Im}S_2$	$\gamma$	$\delta$			
287	$\delta$	$\gamma$	$\delta$	$\gamma$	$\delta$	$\gamma$	$\delta$		
	0	359	183	286	0	359	183	352	147

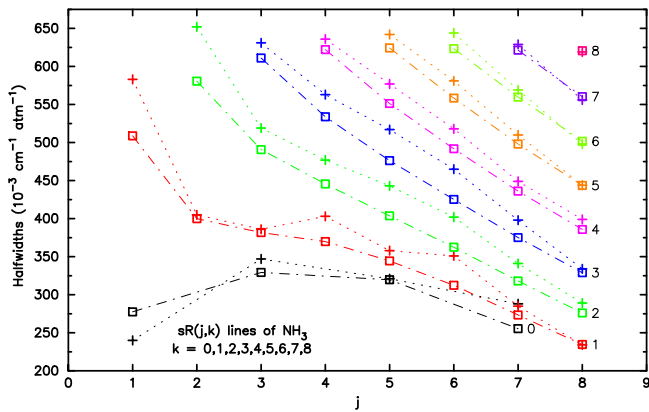


FIG. 9. Calculated half-widths ( $\square$ ) and measured results (+) by Brown and Peterson<sup>21</sup> of  $sR(j,k)$  lines in the pure rotational band. The sub-blocks with  $k \neq 0$  are labeled by their  $k$  values at the right side of  $sR(8,k)$  and the sub-block with  $k = 0$  is labeled on the right side of calculated value of  $sR(7,0)$ .

in the  $\nu_1$  and pure rotational bands for self-broadened  $\text{NH}_3$  point out that for these bands, the significant overestimation mainly results from applying this assumption. We thus believe that different intermolecular interactions induce different behaviours. Because the  $\text{NH}_3$  molecule has a large dipole moment, the leading long-range interaction in  $\text{NH}_3\text{-NH}_3$  collisions is much stronger than that in other systems. As a result, as one carries out an average over the collisional trajectories, glancing collisions make a major contribution. For the other systems, nearly head-on collisions play a major role. On the other hand, the remaining approximation (i.e., neglecting the coupling between the translational and the rotational motions) becomes invalid as two interacting molecules are close. As a result, this remaining invalid approximation does not significantly affect calculated results for  $\text{NH}_3\text{-NH}_3$  at all.

#### D. Comparisons between calculated half-widths and those listed in HITRAN

First of all, by screening values of the air- and self-broadened half-widths for the  $\nu_1$  lines listed in HITRAN 2008 and 2012 with the two symmetry rules mentioned above, we have found that these two data sets exactly follow the second rule. However, the air-broadened half-widths exactly follow the first rule and the self-broadened ones do not follow it at all. The screening result indicates that these two data sets listed in HITRAN are, at least, not consistent.

Secondly, by comparing our calculated half-widths in the  $\nu_1$  band with those in HITRAN 2012, we have found a reasonable agreement in the R branch, that deteriorates in the Q and P branches (see Table IV of the supplementary material<sup>51</sup>). We guess that the empirical formulas<sup>21</sup> used to provide the HITRAN values may play a role here.

#### V. CALCULATED SHIFTS

Because reliable shift measurements are difficult to carry out, those reported in Ref. 22 may contain large uncertainties. With respect to theoretical calculations, the accuracy of

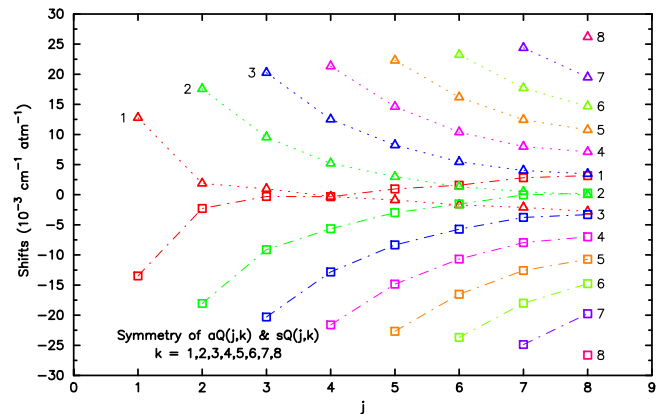


FIG. 10. An approximate symmetry of the calculated shifts for pairs of  $aQ(j,k)$  ( $\square$ ) and  $sQ(j,k)$  ( $\Delta$ ) with  $k = 1, 2, \dots, 8$  in the  $\nu_1$  band. The sub-blocks of  $aQ(j,k)$  are labeled by their  $k$  values at the right side of calculated shifts of  $aQ(8,k)$ . A similar labeling is applied for the sub-block of  $sQ(j,k)$  with  $k \geq 4$ . But, for  $sQ(j,k)$  with  $k \leq 3$ , their  $k$  values are presented on the left side of  $sQ(k,k)$ .

calculated shifts is poorer than that of the half-widths. This results from several factors such as a lot of large cancellations occurring in the calculation process. Moreover, calculated shifts are more sensitive than widths to averaging or not over the Maxwell-Boltzmann distribution of translational energy.<sup>52,53</sup> Since the present work uses the average velocity approximation, no quantitative comparisons between theoretical calculations and measurements is presented here (see supplementary material<sup>51</sup>) and the discussion is limited to more qualitative behaviors.

Indeed, even if limited, our model remains a useful tool that enables one to monitor variations of shift values for most of the  $\text{NH}_3$  lines in the  $\nu_1$  and pure rotational bands. As mentioned in Sec. IV A, there are two approximate rules applicable for the half-width. With more tolerance, similar rules exist also for the shifts. First of all, in Fig. 10 we present calculated shifts for pairs of  $aQ(j,k)$  and  $sQ(j,k)$  with  $k = 1, 2, \dots, 8$  in the  $\nu_1$  band as functions of  $j$ . As expected, the magnitudes of the shifts for doublets are almost identical, but their signs are opposite. In other words, the plot demonstrates

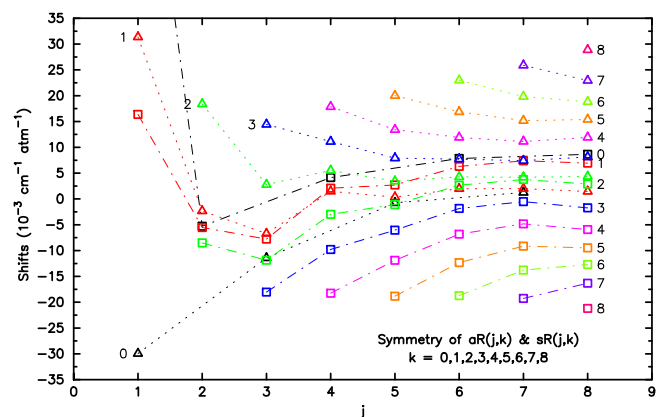


FIG. 11. An approximate symmetry of calculated shifts for doublets of  $aR(j,k)$  ( $\square$ ) and  $sR(j,k)$  ( $\Delta$ ) with  $k = 0, 1, 2, \dots, 8$  in the  $\nu_1$  band. A value of  $183.52 \times 10^{-3} \text{ cm}^{-1} \text{ atm}^{-1}$  for  $aR(0,0)$  is outside of the figure frame. The sub-block labeling is similar to Fig. 10.

that the first rule is approximately valid for the shift. In addition, it is worth mentioning that except for the sub-block with  $k = 1$ , the shifts in the same  $k$  sub-blocks vary smoothly and the variation patterns in different sub-blocks are well organized. This implies that for lines with  $j \geq 9$ , it is possible to predict their shift values based on those available with  $j < 9$ . Of course, lines involving the intramolecular resonances must be excluded.

Secondly, in Fig. 11 we present calculated shifts for doublets of  $aR(j,k)$  and  $sR(j,k)$  with  $k = 0, 1, 2, \dots, 8$  as function of  $j$ . The pair with a specified  $j$  consists of two lines with only switching their initial and final inverse symmetry indices “a” and “s”. As shown by the figure, the “anti-symmetry” is approximately valid for lines in sub-blocks with  $k \geq 3$ . However, the rule is completely broken for  $k = 0, 1$ , and 2. For these lines, the shift values are somehow randomly distributed. A detailed discussion of these behaviors will be our further research subject, as well as a comparison with the experimental data which requires to remove the average velocity approximation.

## VI. CONCLUSION

We have extended the refined RB formalism to the case of symmetric tops with inversion symmetry. In a first step the model has been applied to parallel bands of self-broadened  $\text{NH}_3$ . The very successful comparison of calculated and experimental widths has demonstrated, once more, the importance of line coupling. In the present case, the coupling between the two components of each inversion doublet plays a major (but not unique) role in the reduction of the widths, when compared to the former RB formalism.

The present formalism can be easily extended to foreign gas broadening, for which many experimental results are available. With respect to an extension to perpendicular bands, the situation is more complicated, since the radiative selection rule now is  $\Delta k = \pm 1$  (instead of  $\Delta k = 0$  for the parallel bands) and requires a re-examination of the linespace structure. Furthermore, as in the  $\text{CO}_2$  case,<sup>18</sup> the vibrational angular momentum may play a role.

Besides, among the various extensions of the present work, an interesting challenge should be the comparison of the calculated widths and shifts, and more generally of the entire relaxation matrix for the  $\nu_1$ ,  $\nu_2$ , and  $2\nu_2$  bands. As

shown in the present work, one of the parameters governing the amplitude of the line coupling within doublets is the inversion splitting. However, the latter strongly varies when going from the  $\nu_1 = 1$  level ( $\cong 1 \text{ cm}^{-1}$ ) to the  $\nu_2 = 1$  level ( $\cong 36 \text{ cm}^{-1}$ ) and to the  $\nu_2 = 2$  level ( $\cong 284 \text{ cm}^{-1}$ ). Based on the present analysis, it can be reasonably expected that, when compared to the  $\nu_1$  band, line coupling (and hence line mixing) among doublets will be much smaller in the  $\nu_2$  band and non-existent in the  $2\nu_2$  band.

It must be emphasized that the present formalism, by removing the isolated line approximation, enables the calculation of the entire relaxation matrix. As noted previously the significant reduction of the widths consecutively indicates non-negligible off-diagonal elements of the relaxation matrix. It is therefore interesting to see if the present model could explain the obvious and complex line mixing signatures observed by Pine and Markov in the  $\nu_1$  band.<sup>22</sup> This is the subject of Paper II.<sup>31</sup> Finally, all the calculated complex relaxation matrices in the  $\nu_1$  band are available in the supplementary material.<sup>51</sup>

## ACKNOWLEDGMENTS

The authors would like to thank the reviewers for their valuable suggestions and comments and for greatly improving the manuscript. One of the authors (Q. Ma) acknowledges financial support from NSF under Grant No. 1501297. This research used resources of the National Research Scientific Computing Center, which is supported by the Office of Science of the U.S. Department of Energy under Contract No. DE-AC02-05CH11231.

## APPENDIX A: POTENTIAL MATRIX ELEMENTS IN HILBERT SPACE

In order to derive expressions for the matrix elements of  $S_{2,\text{outer},i}$ ,  $S_{2,\text{outer},f}$ , and  $S_{2,\text{middle}}$ , one needs the potential matrix elements  $\langle i'm'_i i'_2 m'_2 | V(R(t)) | im_i i_2 m_2 \rangle$ . In the presence of inversion symmetries, each of the notations  $i$ ,  $i'$ ,  $i_2$ , and  $i'_2$  represents a summation of two terms. As a result, the matrix elements contain 16 terms with different combinations of  $\pm k$ ,  $\pm k'$ ,  $\pm k_2$ , and  $\pm k'_2$ . For example, for the term with all the positive  $k$  values, we show how to evaluate it in detail here,

$$\begin{aligned} \langle v'_i j'_i k'_i m'_i j'_2 k'_2 m'_2 | V(R(t)) | v_i j_i k_i m_i j_2 k_2 m_2 \rangle &= \delta_{v'_i v_i} \sqrt{(2j'_i + 1)(2j_i + 1)(2j'_2 + 1)(2j_2 + 1)} \sum_{L_1 K_1 L_2 K_2 L} \frac{1}{(2L_1 + 1)(2L_2 + 1)} \\ &\times (-1)^{k_i + k_2} C(j_i j'_i L_1, -k_i k'_i K_1) C(j_2 j'_2 L_2, -k_2 k'_2 K_2) \\ &\times U(L_1 L_2 L; K_1 K_2; R(t)) \sum_{\mu_1 \mu_2 M} (-1)^{m_i + m_2} C(L_1 L_2 L, \mu_1 \mu_2 M) \\ &\times C(j_i j'_i L_1, -m_i m'_i \mu_1) C(j_2 j'_2 L_2, -m_2 m'_2 \mu_2) Y_{LM}^*(\omega(t)). \end{aligned} \quad (\text{A1})$$

Similarly, all the other 15 terms can be obtained and their expressions are almost identical to Eq. (A1). Then, by simply adding them together, one obtains the expression for the potential matrix elements as

$$\begin{aligned}
\langle i'm'_i i'_2 m'_2 | V(R(t)) | im_i i_2 m_2 \rangle &= \delta_{v'v_i} \sqrt{(2j'_i + 1)(2j_i + 1)(2j'_2 + 1)(2j_2 + 1)} \sum_{L_1 K_1 L_2 K_2 L} \frac{1}{(2L_1 + 1)(2L_2 + 1)} \\
&\times D^P(\varepsilon'_i j'_i k'_i, \varepsilon_i j_i k_i; L_1 K_1) D^P(\varepsilon'_2 j'_2 k'_2, \varepsilon_2 j_2 k_2; L_2 K_2) \\
&\times U(L_1 L_2 L; K_1 K_2; R(t)) \sum_{\mu_1 \mu_2 M} (-1)^{m_i + m_2} C(L_1 L_2 L, \mu_1 \mu_2 M) \\
&\times C(j_i j'_i L_1, -m_i m'_i \mu_1) C(j_2 j'_2 L_2, -m_2 m'_2 \mu_2) Y_{LM}^*(\omega(t)), \tag{A2}
\end{aligned}$$

where the  $D^P$  matrix is defined by

$$D^P(\varepsilon' j' k', \varepsilon j k; LK) = N_{\varepsilon'} N_{\varepsilon} (-1)^k \{ C(j j' L, -k k' K) + \varepsilon' C(j j' L, -k - k' K) + \varepsilon C(j j' L, k k' K) + \varepsilon \varepsilon' C(j j' L, k - k' K) \}. \tag{A3}$$

In the notation of  $D^P$ , the superscript of  $P$  is used to emphasize a parity specification. By comparing Eqs. (A1) and (A2), their differences are replacements of  $(-1)^{k_i} C(j_i j'_i L_1, -k_i k'_i K_1)$  by  $D^P(\varepsilon'_i j'_i k'_i, \varepsilon_i j_i k_i; L_1 K_1)$  and  $(-1)^{k_2} C(j_2 j'_2 L_2, -k_2 k'_2 K_2)$  by  $D^P(\varepsilon'_2 j'_2 k'_2, \varepsilon_2 j_2 k_2; L_2 K_2)$ .

## APPENDIX B: DERIVATIONS OF EXPRESSIONS FOR $S_{2,outer,i}^{i'f',if}$ , $S_{2,outer,f}^{i'f',if}$ , AND $S_{2,middle}^{i'f',if}$

The expression for matrix elements of  $S_{2,outer,i}$  is given by<sup>10</sup>

$$\begin{aligned}
S_{2,outer,i}^{i'f',if}(r_c) &= \frac{1}{\hbar^2} \int_{-\infty}^{\infty} dt \int_{-\infty}^t dt' \langle \langle i' f', J M_J | \langle L_1(t) L_1(t') | i f, J M_J \rangle \rangle_{outer,i} \\
&= \frac{\delta_{j'_i j_i} \delta_{f f'}}{\hbar^2 (2j_i + 1)} \int_{-\infty}^{\infty} dt \int_{-\infty}^t dt' \sum_{i_2} \sqrt{\rho_{i_2} \rho_{i'_2}} \sum_{i''} \sum_{i'_2} \sum_{(m)} e^{i(\omega_{i''} + \omega_{i_2 i'_2})t - i(\omega_{i''} + \omega_{i_2 i'_2})t'} \\
&\times \langle i' m_i i_2 m_2 | V(R(t)) | i'' m''_i i'_2 m'_2 \rangle \langle i'' m''_i i'_2 m'_2 | V(R(t')) | im_i i_2 m_2 \rangle. \tag{B1}
\end{aligned}$$

In Eq. (B1),  $\omega_{i i'} = [E^{(a)}(i) - E^{(a)}(i')]/\hbar$ ,  $\omega_{i_2 i'_2} = [E^{(b)}(i_2) - E^{(b)}(i'_2)]/\hbar$ , and the superscripts of (a) and (b) are used to indicate the absorber and bath molecules, respectively. We note that due to a presence of the factor of  $\delta_{j'_i j_i}$  in Eq. (B1), the off-diagonal elements of  $S_{2,outer,i}$  have non-zero values only among those lines with the same angular values. For linear molecules, this implies that the  $S_{2,outer,i}$  term is diagonal in the line space within the same bands. For more complicated molecules, the  $S_{2,outer,i}$  term can have non-zero off-diagonal elements within the same bands, but they are confined within sub-blocks of the line space.

With Eq. (A2), off-diagonal elements  $S_{2,outer,i}$  (i.e., Eq. (B1)) can be expressed as

$$\begin{aligned}
S_{2,outer,i}^{i'f',if}(r_c) &= \frac{\delta_{j'_i j_i} \delta_{f f'}}{\hbar^2} \sum_{i_2 i'_2} \sqrt{\rho_{i_2} \rho_{i'_2}} (2j_2 + 1)(2j'_2 + 1) \\
&\times \sum_{L_1 K_1 L_2 K_2 L} \sum_{L'_1 K'_1 L'_2 K'_2 L'} \frac{D^P(\varepsilon_2 j_2 k_2, \varepsilon'_2 j'_2 k'_2; L_2 K_2) D^P(\varepsilon'_2 j'_2 k'_2, \varepsilon_2 j_2 k_2; L'_2 K'_2)}{(2L_1 + 1)(2L_2 + 1)(2L'_1 + 1)(2L'_2 + 1)} \\
&\times \sum_{\varepsilon'' j''_i k''_i} (2j''_i + 1) D^P(\varepsilon'_i j'_i k'_i, \varepsilon''_i j''_i k''_i; L_1 K_1) D^P(\varepsilon''_i j''_i k''_i, \varepsilon_i j_i k_i; L'_1 K'_1) \int_{-\infty}^{\infty} dt \int_{-\infty}^t dt' e^{i(\omega_{i''} + \omega_{i_2 i'_2})t - i(\omega_{i''} + \omega_{i_2 i'_2})t'} \\
&\times U(L_1 L_2 L; K_1 K_2; R(t)) U(L'_1 L'_2 L'; K'_1 K'_2; R(t')) \sum_{(m)} (-1)^{m''_i + m'_2 + m_i + m_2} \\
&\times C(L_1 L_2 L, \mu_1 \mu_2 M) C(L'_1 L'_2 L', \mu_1 \mu_2 M) C(j''_i j_i L_1, -m''_i m_i \mu_1) C(j_i j'_i L_1, -m_i m'_i \mu_1) \\
&\times C(j'_2 j_2 L_2, -m'_2 m_2 \mu_2) C(j_2 j'_2 L'_2, -m_2 m'_2 \mu_2) Y_{LM}^*(\omega(t)) Y_{L'M'}^*(\omega(t')). \tag{B2}
\end{aligned}$$

By carrying out the summations over the magnetic quantum numbers in Eq. (B2), one obtains three Kronecker deltas of  $\delta_{L_1 L'_1}$ ,  $\delta_{L_2 L'_2}$ , and  $\delta_{L_1 L'_1}$ . Then, by introducing the two dimensional (2-D) correlation functions  $G_{L_1 K_1 K'_1 L_2 K_2 K'_2}(t, t')$  defined by

$$\begin{aligned}
G_{L_1 K_1 K'_1 L_2 K_2 K'_2}(t, t') &= \frac{1}{4\pi \hbar^2 (2L_1 + 1)^2 (2L_2 + 1)^2} \sum_L (-1)^{L_1 + L_2 + L} \\
&\times (2L + 1) U(L_1 L_2 L; K_1 K_2; R(t)) U(L_1 L_2 L; K'_1 K'_2; R(t')) P_L[\Theta(t, t')], \tag{B3}
\end{aligned}$$

where  $\Theta(t, t')$  is the angle between  $\vec{R}(t)$  and  $\vec{R}(t')$ , one can rewrite Eq. (B2),

$$\begin{aligned}
 S_{2,outer,i}^{i'f',if}(r_c) &= \delta_{j'_i j_i} \delta_{f'f} \sum_{L_1 K_1 K'_1 L_2 K_2 K'_2} \sum_{\varepsilon'_i j'_i k'_i} (2j'_i + 1) \\
 &\times D^P(\varepsilon'_i j'_i k'_i, \varepsilon''_i j''_i k''_i; L_1 K_1) D^P(\varepsilon''_i j''_i k''_i, \varepsilon_i j_i k_i; L_1 K_1) \sum_{i_2 i'_2} \sqrt{\rho_{i_2} \rho_{i'_2}} (2j_2 + 1) \\
 &\times (2j'_2 + 1) D^P(\varepsilon_2 j_2 k_2, \varepsilon'_2 j'_2 k'_2; L_2 K_2) D^P(\varepsilon'_2 j'_2 k'_2, \varepsilon_2 j_2 k_2; L_2 K_2) \\
 &\times \int_{-\infty}^{\infty} dt \int_{-\infty}^t dt' e^{i(\omega_{i'f'} + \omega_{i_2 i'_2})t - i(\omega_{if} + \omega_{i_2 i_2})t'} G_{L_1 K_1 K'_1 L_2 K_2 K'_2}(t, t'). \tag{B4}
 \end{aligned}$$

In terms of the symmetric 2-D Fourier and Hilbert transforms of  $\mathbb{F}_{L_1 K_1 K'_1 L_2 K_2 K'_2}(\omega, \omega')$  and  $\mathbb{H}_{L_1 K_1 K'_1 L_2 K_2 K'_2}(\omega, \omega')$  defined by Eqs. (C3) and (C4), respectively, the integrations over  $t$  and  $t'$  appearing in Eq. (B4) can be evaluated by Eq. (C3). Then, the expression for the real part of  $S_{2,outer,i}^{i'f',if}(r_c)$  is given by

$$\begin{aligned}
 ReS_{2,outer,i}^{i'f',if}(r_c) &= \pi \delta_{j'_i j_i} \delta_{f'f} \sum_{L_1 K_1 K'_1 L_2 K_2 K'_2} \sum_{\varepsilon'_i j'_i k'_i} (2j'_i + 1) \\
 &\times D^P(\varepsilon'_i j'_i k'_i, \varepsilon''_i j''_i k''_i; L_1 K_1) D^P(\varepsilon''_i j''_i k''_i, \varepsilon_i j_i k_i; L_1 K_1) \sum_{i_2 i'_2} \sqrt{\rho_{i_2} \rho_{i'_2}} (2j_2 + 1) \\
 &\times (2j'_2 + 1) D^P(\varepsilon_2 j_2 k_2, \varepsilon'_2 j'_2 k'_2; L_2 K_2) D^P(\varepsilon'_2 j'_2 k'_2, \varepsilon_2 j_2 k_2; L_2 K_2) \mathbb{F}_{L_1 K_1 K'_1 L_2 K_2 K'_2} \left( \frac{\omega_{i'f'} + \omega_{i_2 i'_2}}{2} + \omega_{i_2 i_2}, \omega_{if} \right). \tag{B5}
 \end{aligned}$$

The expression for the imaginary part of  $S_{2,outer,i}^{i'f',if}(r_c)$  is the same as Eq. (B5) except that  $\mathbb{F}_{L_1 K_1 K'_1 L_2 K_2 K'_2}$  are replaced by  $\mathbb{H}_{L_1 K_1 K'_1 L_2 K_2 K'_2}$ . Similarly, the expression of  $ReS_{2,outer,f}^{i'f',if}(r_c)$  can be obtained from Eq. (B5) by making exchanges between the quantum numbers  $i$  and  $f'$  and between  $i'$  and  $f$ . The

expression for  $ImS_{2,outer,f}^{i'f',if}(r_c)$  can also be obtained from  $ReS_{2,outer,f}^{i'f',if}(r_c)$  through similar replacements. In addition, all the conclusions for  $S_{2,outer,i}$  are also valid for  $S_{2,outer,f}$ .

For matrix elements of  $S_{2,middle}^{i'f',if}$ , the starting expression is given by<sup>10</sup>

$$\begin{aligned}
 S_{2,middle}^{i'f',if}(r_c) &= -\frac{1}{\hbar^2(2J+1)} \int_{-\infty}^{\infty} dt \int_{-\infty}^{\infty} dt' \sum_{i_2} \sqrt{\rho_{i_2} \rho_{i'_2}} \sum_{i'_2} \sum_{(m)} e^{i(\omega_{i'i} + \omega_{i'_2 i'_2})t - i(\omega_{f'f} + \omega_{i'_2 i_2})t'} \\
 &\times (-1)^{j_f - m_f + j'_f - m'_f} C(j'_i j'_f J, m'_i - m'_f M_J) C(j_i j_f J, m_i - m_f M_J) \\
 &\times \langle i' m'_i i'_2 m'_2 | V(R(t)) | i m_i i_2 m_2 \rangle \langle f m_f i_2 m_2 | V(R(t')) | f' m'_f i'_2 m'_2 \rangle. \tag{B6}
 \end{aligned}$$

Similarly, by applying Eq. (A2) and carrying the summations over the magnetic quantum numbers, Eq. (B6) becomes

$$\begin{aligned}
 S_{2,middle}^{i'f',if}(r_c) &= (-1)^{1+J} \delta_{v'_i v_i} \delta_{v'_f v_f} (-1)^{j_f + j'_f} \\
 &\times \sqrt{(2j'_i + 1)(2j'_f + 1)(2j_i + 1)(2j_f + 1)} \sum_{L_1 K_1 K'_1 L_2 K_2 K'_2} (-1)^{L_1} W(j'_i j'_f j_i j_f, J L_1) \\
 &\times D^P(\varepsilon'_i j'_i k'_i, \varepsilon_i j_i k_i; L_1 K_1) D^P(\varepsilon_f j_f k_f, \varepsilon'_f j'_f k'_f; L_1 K_1) \sum_{i_2 i'_2} \sqrt{\rho_{i_2} \rho_{i'_2}} \\
 &\times (2j_2 + 1)(2j'_2 + 1) D^P(\varepsilon'_2 j'_2 k'_2, \varepsilon_2 j_2 k_2; L_2 K_2) D^P(\varepsilon_2 j_2 k_2, \varepsilon'_2 j'_2 k'_2; L_2 K_2) \\
 &\times \int_{-\infty}^{\infty} dt \int_{-\infty}^{\infty} dt' e^{i(\omega_{i'i} + \omega_{i'_2 i'_2})t} e^{-i(\omega_{f'f} + \omega_{i'_2 i_2})t'} G_{L_1 K_1 K'_1 L_2 K_2 K'_2}(t, t'). \tag{B7}
 \end{aligned}$$

As shown in Eq. (C5), the two dimensional integrations over  $t$  and  $t'$  can be evaluated through the 2-D Fourier transforms of  $\mathbb{F}_{L_1K_1K'_1L_2K_2K'_2}(\omega, \omega')$ . Then, one obtains a general expression for  $S_{2,middle}^{i'f',if}$  as

$$\begin{aligned} S_{2,middle}^{i'f',if}(r_c) &= 2\pi(-1)^{1+J} \delta_{\nu_i' \nu_i} \delta_{\nu_f' \nu_f} (-1)^{J_f+J_f'} \\ &\times \sqrt{(2j_i'+1)(2j_f'+1)(2j_i+1)(2j_f+1)} \sum_{L_1K_1K'_1L_2K_2K'_2} (-1)^{L_1} W(j_i' j_f' j_i j_f, JL_1) \\ &\times D^P(\varepsilon_i' j_i' k_i', \varepsilon_i j_i k_i; L_1 K_1) D^P(\varepsilon_f j_f k_f, \varepsilon_f' j_f' k_f'; L_1 K_1') \sum_{i_2 i_2'} \sqrt{\rho_{i_2} \rho_{i_2'}} \\ &\times (2j_2+1)(2j_2'+1) D^P(\varepsilon_2' j_2' k_2', \varepsilon_2 j_2 k_2; L_2 K_2) D^P(\varepsilon_2 j_2 k_2, \varepsilon_2' j_2' k_2'; L_2 K_2') \\ &\times \mathbb{F}_{L_1K_1K'_1L_2K_2K'_2} \left( \frac{\omega_{i_i'} + \omega_{f_f'}}{2} + \omega_{i_2' i_2}, \omega_{f_i} - \omega_{f_i'} \right). \end{aligned} \quad (B8)$$

For the diagonal elements of  $S_{2,outer,i}$ ,  $S_{2,outer,f}$ , and  $S_{2,middle}$ , their expressions become simpler because the second arguments of the symmetric 2-D Fourier and Hilbert transforms  $\mathbb{F}_{L_1K_1K'_1L_2K_2K'_2}$  and  $\mathbb{H}_{L_1K_1K'_1L_2K_2K'_2}$  are zero. With Eqs. (C9) and (C10), one can directly obtain them from Eqs. (B5) and (B8) by replacing these 2-D functions by their corresponding 1-D partners. We note that to simplify the notations, we have used the same symbols denoted for these 2-D and 1-D functions, but with different numbers of their arguments.

### APPENDIX C: SYMMETRIC 2-D AND 1-D CORRELATION FUNCTIONS AND THEIR FOURIER TRANSFORMS

As explained in our previous work,<sup>17</sup> instead of introducing the 2-D correlation functions  $G_{L_1K_1K'_1L_2K_2K'_2}(t, t')$  defined by Eq. (B3), it is better to change the variables  $t$  and  $t'$  to the variables of  $\tau \equiv t - t'$  and  $\tau' \equiv 1/2(t + t')$  and to use their

symmetric partners  $\mathbb{G}_{L_1K_1K'_1L_2K_2K'_2}(\tau, \tau')$  defined by

$$\mathbb{G}_{L_1K_1K'_1L_2K_2K'_2}(\tau, \tau') = G_{L_1K_1K'_1L_2K_2K'_2} \left( \tau' + \frac{\tau}{2}, \tau' - \frac{\tau}{2} \right). \quad (C1)$$

One can therefore express the off-diagonal elements of  $S_{2,outer,i}$ ,  $S_{2,outer,f}$ , and  $S_{2,middle}$  in terms of the symmetric 2-D Fourier transforms defined by

$$\begin{aligned} \mathbb{F}_{L_1K_1K'_1L_2K_2K'_2}(\omega, \omega') &= \frac{1}{2\pi} \int_{-\infty}^{\infty} \int_{-\infty}^{\infty} d\tau d\tau' e^{i\omega\tau} e^{i\omega'\tau'} \mathbb{G}_{L_1K_1K'_1L_2K_2K'_2}(\tau, \tau'). \end{aligned} \quad (C2)$$

Because  $\mathbb{G}_{L_1K_1K'_1L_2K_2K'_2}(\tau, \tau')$  are even functions of  $\tau$  and  $\tau'$ , these Fourier transforms are real and even functions of  $\omega$  and  $\omega'$ .

For example, the integrations over  $t$  and  $t'$  appearing in Eq. (B4) can be evaluated as

$$\begin{aligned} \int_{-\infty}^{\infty} dt \int_{-\infty}^t dt' e^{i(\omega_{i_i''} + \omega_{i_2' i_2})t - i(\omega_{i_i''} + \omega_{i_2' i_2})t'} G_{L_1K_1K'_1L_2K_2K'_2}(t, t') &= \int_{-\infty}^{\infty} d\tau' \int_0^{\infty} d\tau e^{i\omega_{i_i''} \tau + i \left( \frac{\omega_{i_i''} + \omega_{i_2' i_2}}{2} + \omega_{i_2' i_2} \right) \tau} \mathbb{G}_{L_1K_1K'_1L_2K_2K'_2}(\tau, \tau') \\ &= \pi \mathbb{F}_{L_1K_1K'_1L_2K_2K'_2} \left( \frac{\omega_{i_i''} + \omega_{i_2' i_2}}{2} + \omega_{i_2' i_2}, \omega_{i_i''} \right) + i\pi \mathbb{H}_{L_1K_1K'_1L_2K_2K'_2} \left( \frac{\omega_{i_i''} + \omega_{i_2' i_2}}{2} + \omega_{i_2' i_2}, \omega_{i_i''} \right). \end{aligned} \quad (C3)$$

In Eq. (C3),  $\mathbb{H}_{L_1K_1K'_1L_2K_2K'_2}(\omega, \omega')$  are the Hilbert transforms of  $\mathbb{F}_{L_1K_1K'_1L_2K_2K'_2}(\omega, \omega')$  over the first argument  $\omega$ ,

$$\mathbb{H}_{L_1K_1K'_1L_2K_2K'_2}(\omega, \omega') = \frac{1}{\pi} P \int_{-\infty}^{\infty} d\omega'' \frac{1}{\omega - \omega''} \mathbb{F}_{L_1K_1K'_1L_2K_2K'_2}(\omega'', \omega'). \quad (C4)$$

$\mathbb{H}_{L_1K_1K'_1L_2K_2K'_2}(\omega, \omega')$  are real, odd functions of  $\omega$  and even functions of  $\omega'$ .

Deriving the expression for two dimensional integrations over  $t$  and  $t'$  appearing in Eq. (B7) can be handled with a similar way. In this case, because both the integration ranges of  $t$  and  $t'$  are from  $-\infty$  to  $+\infty$ , the result is real,

$$\int_{-\infty}^{\infty} dt \int_{-\infty}^{\infty} dt' e^{i(\omega_{i_i'} + \omega_{i_2' i_2})t} e^{-i(\omega_{f_f'} + \omega_{i_2' i_2})t'} G_{L_1K_1K'_1L_2K_2K'_2}(t, t') = 2\pi \mathbb{F}_{L_1K_1K'_1L_2K_2K'_2} \left( \frac{\omega_{i_i'} + \omega_{f_f'}}{2} + \omega_{i_2' i_2}, \omega_{f_i} - \omega_{f_i'} \right). \quad (C5)$$

It is worth mentioning that as one calculates the diagonal matrix elements of  $S_{2, \text{outer}, i}$ ,  $S_{2, \text{outer}, f}$ , and  $S_{2, \text{middle}}$ , the integrations over  $t$  and  $t'$  becomes simpler. In these cases, one introduces the symmetric 1-D correlation functions  $\mathbb{G}_{L_1 K_1 K'_1 L_2 K_2 K'_2}(\tau)$ ,

$$\mathbb{G}_{L_1 K_1 K'_1 L_2 K_2 K'_2}(\tau) = \int_{-\infty}^{\infty} d\tau' \mathbb{G}_{L_1 K_1 K'_1 L_2 K_2 K'_2}(\tau, \tau'). \quad (\text{C6})$$

It is obvious that the 1-D functions of  $\mathbb{G}_{L_1 K_1 K'_1 L_2 K_2 K'_2}(\tau)$  are even functions of  $\tau$ . For simplifying notations, we use the same symbols to represent the 2-D and 1-D correlation functions. Meanwhile, their corresponding Fourier and Hilbert transforms are defined by

$$\mathbb{F}_{L_1 K_1 K'_1 L_2 K_2 K'_2}(\omega) = \frac{1}{\sqrt{2\pi}} \int_{-\infty}^{\infty} d\tau e^{i\omega\tau} \mathbb{G}_{L_1 K_1 K'_1 L_2 K_2 K'_2}(\tau), \quad (\text{C7})$$

and

$$\mathbb{H}_{L_1 K_1 K'_1 L_2 K_2 K'_2}(\omega) = \frac{1}{\pi} P \int_{-\infty}^{\infty} d\omega' \frac{1}{\omega - \omega'} \mathbb{F}_{L_1 K_1 K'_1 L_2 K_2 K'_2}(\omega'), \quad (\text{C8})$$

where  $P$  means the Cauchy principle value. It is easy to show that there are simple relations between these 2-D and 1-D transforms as

$$\mathbb{F}_{L_1 K_1 K'_1 L_2 K_2 K'_2}(\omega, 0) = \frac{1}{\sqrt{2\pi}} \mathbb{F}_{L_1 K_1 K'_1 L_2 K_2 K'_2}(\omega), \quad (\text{C9})$$

and

$$\mathbb{H}_{L_1 K_1 K'_1 L_2 K_2 K'_2}(\omega, 0) = \frac{1}{\sqrt{2\pi}} \mathbb{H}_{L_1 K_1 K'_1 L_2 K_2 K'_2}(\omega). \quad (\text{C10})$$

It is worth mentioning that these 2-D and 1-D functions play crucial roles in calculating the relaxation matrix elements. Meanwhile, calculating them for each collisional trajectories governed by an accurate potential model is the most time-consuming task in practical calculations.

<sup>1</sup>J. M. Hartmann, C. Boulet, and D. Robert, *Collisional Effects on Molecular Spectra. Laboratory Experiments and Models. Consequences for Applications* (Elsevier, 2008).

<sup>2</sup>L. S. Rothman, I. E. Gordon, Y. Babikov *et al.*, *J. Quant. Spectrosc. Radiat. Transfer* **130**, 4 (2013).

<sup>3</sup>R. G. Gordon, *J. Chem. Phys.* **44**, 3083 (1966); **45**, 1649 (1966).

<sup>4</sup>C. J. Tsao and B. Curnutte, *J. Quant. Spectrosc. Radiat. Transfer* **2**, 41 (1962).

<sup>5</sup>S. Green, *J. Chem. Phys.* **62**, 2271 (1975).

<sup>6</sup>K. S. Lam, *J. Quant. Spectrosc. Radiat. Transfer* **17**, 351 (1977).

<sup>7</sup>D. Robert and J. Bonamy, *J. Phys.* **40**, 923 (1979).

<sup>8</sup>P. W. Anderson, *Phys. Rev.* **76**, 647 (1949).

<sup>9</sup>J. Buldyreva, N. N. Lavrentieva, and V. I. Starikov, *Collisional Line Broadening and Shifting at Atmospheric Gases: A Practical Guide for Line Shape Modelling by Current Semi-Classical Approaches* (Imperial College Press, 2011).

<sup>10</sup>Q. Ma, C. Boulet, and R. H. Tipping, *J. Chem. Phys.* **139**, 034305 (2013).

<sup>11</sup>M. Afzelius, P. Bengtsson, and J. Bonamy, *J. Chem. Phys.* **120**, 8616 (2004).

<sup>12</sup>F. Thibault, L. Gomez, S. V. Ivanov, O. G. Buzynkin, and C. Boulet, *J. Quant. Spectrosc. Radiat. Transfer* **113**, 1887 (2012), and references therein.

<sup>13</sup>G. Buffa and O. Tarrini, *Phys. Rev. A* **16**, 1612 (1977).

<sup>14</sup>G. Cazzoli, L. Cludi, G. Cotti, C. Degli Esposti, G. Buffa, and O. Tarrini, *J. Chem. Phys.* **102**, 1149 (1995).

<sup>15</sup>Q. Ma, R. H. Tipping, and C. Boulet, *J. Quant. Spectrosc. Radiat. Transfer* **103**, 588 (2007).

<sup>16</sup>C. Boulet, Q. Ma, and F. Thibault, *J. Chem. Phys.* **140**, 084310 (2014).

<sup>17</sup>Q. Ma, C. Boulet, and R. H. Tipping, *J. Chem. Phys.* **140**, 104304 (2014).

<sup>18</sup>C. Boulet, Q. Ma, and R. H. Tipping, *J. Chem. Phys.* **143**, 124313 (2015).

<sup>19</sup>Q. Ma, C. Boulet, and R. H. Tipping, *J. Chem. Phys.* **140**, 244301 (2014).

<sup>20</sup>V. N. Markov, A. S. Pine, G. Buffa, and O. Tarrini, *J. Quant. Spectrosc. Radiat. Transfer* **50**, 167 (1993).

<sup>21</sup>L. R. Brown and D. B. Peterson, *J. Mol. Spectrosc.* **168**, 593 (1994).

<sup>22</sup>A. S. Pine and V. N. Markov, *J. Quant. Spectrosc. Radiat. Transfer* **228**, 121 (2004).

<sup>23</sup>G. Baldacchini, G. Buffa, F. d'Amato, O. Tarrini, M. De Rosa, and F. Pelagalli, *J. Quant. Spectrosc. Radiat. Transfer* **67**, 365 (2000).

<sup>24</sup>M. Dhib, J. P. Bouanich, H. Aroui, and M. Broquier, *J. Mol. Spectrosc.* **202**, 83 (2000).

<sup>25</sup>S. Haddad, H. Aroui, J. Orphal, J. P. Bouanich, and J. M. Hartmann, *J. Mol. Spectrosc.* **210**, 275 (2001).

<sup>26</sup>H. Aroui, H. Laribi, J. Orphal, and P. Chelin, *J. Quant. Spectrosc. Radiat. Transfer* **110**, 2037 (2009), and references therein.

<sup>27</sup>M. Dhib, M. A. Echargui, H. Aroui, J. Orphal, and J. M. Hartmann, *J. Mol. Spectrosc.* **233**, 138 (2005).

<sup>28</sup>G. Buffa and O. Tarrini, *J. Mol. Spectrosc.* **101**, 271 (1983).

<sup>29</sup>G. Baldacchini, S. Marchetti, V. Montelatici, G. Buffa, and O. Tarrini, *J. Chem. Phys.* **76**, 5271 (1982).

<sup>30</sup>M. Dhib, J. P. Bouanich, H. Aroui, and A. Picard-Bersellini, *J. Quant. Spectrosc. Radiat. Transfer* **68**, 163 (2001).

<sup>31</sup>C. Boulet and Q. Ma, *J. Chem. Phys.* **144**, 224304 (2016).

<sup>32</sup>M. R. Cherkasov, *J. Quant. Spectrosc. Radiat. Transfer* **141**, 73 (2014).

<sup>33</sup>M. R. Cherkasov, *J. Quant. Spectrosc. Radiat. Transfer* **141**, 89 (2014).

<sup>34</sup>S. Green, *J. Chem. Phys.* **73**, 2740 (1980).

<sup>35</sup>A. Ben Reuven, *Phys. Rev.* **145**, 7 (1966).

<sup>36</sup>C. G. Gray and K. E. Gubbins, *Theory of Molecular Fluids* (Oxford University Press, Oxford, 1984).

<sup>37</sup>A. D. Bykov, N. N. Lavrentiva, and L. N. Sinita, *Atmos. Oceanic Opt.* **5**, 587 (1992).

<sup>38</sup>P. Joubert, J. Bonamy, and D. Robert, *J. Quant. Spectrosc. Radiat. Transfer* **61**, 19 (1999).

<sup>39</sup>Q. Ma, R. H. Tipping, C. Boulet, F. Thibault, and J. Bonamy, *J. Mol. Spectrosc.* **243**, 105 (2007).

<sup>40</sup>S. Belli, G. Buffa, and O. Tarrini, *Phys. Rev. A* **55**, 183 (1997).

<sup>41</sup>S. Urban, *J. Quant. Spectrosc. Radiat. Transfer* **48**, 675 (1992).

<sup>42</sup>M. J. Down, C. Hill, S. N. Yurchenko, J. Tennyson, L. R. Brown, and I. Kleiner, *J. Quant. Spectrosc. Radiat. Transfer* **130**, 260 (2013).

<sup>43</sup>S. Urban, R. D'Cunha, K. N. Rao, and D. Papousek, *Can. J. Phys.* **62**, 1775 (1984).

<sup>44</sup>R. Angstl, H. Finsterholz, H. Frunder, D. Illig, D. Papousek, P. Pracna, K. N. Rao, H. W. Schrotter, and S. Urban, *J. Mol. Spectrosc.* **114**, 454 (1985).

<sup>45</sup>M. D. Marshall, K. C. Izqi, and J. S. Muentner, *J. Chem. Phys.* **107**, 1037 (1997).

<sup>46</sup>A. J. Russell and M. A. Spackman, *Mol. Phys.* **84**, 1239 (1995).

<sup>47</sup>J. Komasa and A. J. Thakkar, *Mol. Phys.* **78**, 1039 (1993).

<sup>48</sup>Q. Ma, R. H. Tipping, and C. Boulet, *J. Chem. Phys.* **124**, 014109 (2006).

<sup>49</sup>J. P. Bouanich, H. Aroui, S. Nouri, and A. Picard-Bersellini, *J. Mol. Spectrosc.* **206**, 104 (2001).

<sup>50</sup>Q. Ma, R. H. Tipping, and N. N. Lavrentieva, *J. Quant. Spectrosc. Radiat. Transfer* **113**, 936 (2013).

<sup>51</sup>See supplementary material at <http://dx.doi.org/10.1063/1.4952995> for detailed comparisons of calculated and experimental widths and shifts together with all the calculated complex relaxation matrices in the  $\nu_1$  band.

<sup>52</sup>B. S. Frost, *J. Phys. B: At. Mol. Phys.* **9**, 1001 (1976).

<sup>53</sup>C. Boulet and A. Rosenberg, *J. Phys.* **42**, 203 (1981).